atmosphere

MDPI

Article

A Relationship between Changes of Surface Air and Sea Floor Temperatures at the Arctic Shelf from the Coupled Models Intercomparison Project, Phase 6 Data

Valentina V. Malakhova [1,2,*] and Alexey V. Eliseev [2,3,4,*]

[1] Institute of Computational Mathematics and Mathematical Geophysics, Siberian Branch of the Russian Academy of Sciences, Novosibirsk 630090, Russia
[2] Physical Faculty, Lomonosov Moscow State University, Moscow 119991, Russia
[3] A.M. Obukhov Institute of Atmospheric Physics, Russian Academy of Sciences, Moscow 119017, Russia
[4] Institute of Environmental Sciences, Kazan Federal University, Kazan 420008, Russia
* Correspondence: malax@sscc.ru (V.V.M.); eliseev.alexey.v@mail.ru (A.V.E.)

Abstract: The sensitivity of seafloor temperature T_B to the warming of surface air temperature T_a is examined for 1850–2300, based on simulations with five models from the Coupled Models Intercomparison Project phase 6 ensemble and driven by a scenario with high anthropogenic emissions of greenhouse gases. In this historical period (until 2015), sensitivity coefficients $\varkappa = \Delta T_B / \Delta T_a$ (Δ indicates changes relative to the pre-industrial period) were typically $\leq$0.12 for annual means and up to 0.43 in summer. However, during the same period in the Barents Sea sector, the sensitivity coefficients were as large as 0.6 in summer. For summer, the obtained results are consistent with the limited measurements available for the Siberian shelf. In future, sensitivity coefficients will increase markedly, and $\varkappa \geq 0.7$ will become common for the part of the Arctic shelf that becomes ice-free in summer. Our results have implications for estimating the future thermal state of subsea sediments, as well as for oceanic biota.

Keywords: Arctic shelf; seafloor temperature modeling; CMIP6; future warming

Citation: Malakhova, V.V.; Eliseev, A.V. A Relationship between Changes of Surface Air and Sea Floor Temperatures at the Arctic Shelf from the Coupled Models Intercomparison Project, Phase 6 Data. *Atmosphere* **2023**, *14*, 1024. https://doi.org/10.3390/atmos14061024

Academic Editor: Dae Il Jeong

Received: 25 April 2023
Revised: 6 June 2023
Accepted: 9 June 2023
Published: 14 June 2023

1. Introduction

In the Arctic, surface air temperature (SAT) increases at a rate which is two- or even four-fold faster than the global mean warming—a phenomenon that is referred to as Arctic amplification [1–3]. Despite this, knowledge about the respective temperature changes in the Arctic Ocean (in particular, over the shelf and near the seafloor) remains controversial.

On the one hand, one may argue that the near-floor temperature response to SAT variations would be damped markedly. A respective mechanism is due to the existence of a temperature point at which the water density is at the maximum. For typical Arctic Ocean salinities, from 28 to 34 practical salinity units, this temperature point is from -1 °C to -2 °C and is close to the freezing temperature. Cold and heavy water sinks to the bottom, maintaining a close-to-constant temperature near the seafloor. This might have been the reason for the very small (basically, $\leq$1 °C) temperature increase obtained in [4] for the yearly atmospheric CO_2 content (q_{CO_2}) doubling in the CMIP3 (Coupled Models Intercomparison Project, phase 3) simulations with a 1% of q_{CO_2} increase per year. A somewhat similar result was obtained for CMIP5 (CMIP, phase 5): under the Representative Concentration Pathway 8.5 (RCP8.5), despite very pronounced surface air warming over the Arctic shelf (about 10 °C in 2081–2100 relative to 1986–2005, see Figure 12.11 from [5]), where the near-floor oceanic temperature only increased by (2.3 ± 1.0) °C [6], which is four-fold smaller. Note, however, that the maximum density argument for close-to-constant temperature near the seafloor could be challenged by taking into account oceanic circulation and salinity changes.

On the other hand, it was noted in [7] that, based on oceanic reanalysis data and on the CMIP6 (CMIP, phase 6; see [8]) simulations, water in the Arctic Ocean warms markedly

faster relative to the global mean oceanic temperature at the same depths. This warming could be as large as 6 °C in 2081–2100 relative to 1981–2000 in the layer 0–700 m. However, the most warming is exhibited in the Barents Sea, with smaller temperature changes in other Arctic shelf basins. In addition, sea water temperature changes in the more distant future are not considered in [7]. We note that, despite the oceanic layer from the surface down to the 150 m depth being studied explicitly in the latter paper, Shu et al. estimated the ratio between the temperature change in the Arctic Ocean relative to the globally averaged respective change at the same depth. Thus, the relationships between the warming at different depths in the Arctic Ocean were not considered explicitly in [7].

In addition, sparse measurements of seafloor temperature T_B are available for the summers (from June to September) 1985–2009 [9]. According to the reported results, water in the coastal zone (defined in [9] as a part of the ocean with depths $\leq$ 10 m) warmed by 2.1 °C in the Laptev Sea and by 2.2 °C in the East Siberian Sea. The corresponding surface air temperature, T_a, increases were 2.6 °C and 2.8 °C. Thus, for this particular season and for this particular time interval, $\Delta T_B/\Delta T_a \approx 0.8$, which is rather close to unity. Here, Δ stays for changes of both variables. At the inner shelf (defined in [9] as a part of the ocean with depths greater than 10 m and less than 50 m), the Laptev Sea warming was only 0.8 °C and cooling by 0.25 °C was exhibited in the East Siberian Sea. Therefore, $\Delta T_B/\Delta T_a \approx 0.4$ in this part of the Laptev Sea, and the corresponding $\Delta T_B/\Delta T_a$ in the East Siberian Sea was negative. No measurements at the deeper oceanic regions, or in other parts of the Arctic shelf (neither European nor North American), or in other season were reported in [9].

One of the possible reasons for such controversy in model outputs is the too-coarse resolution of oceanic compartments employed in the previous (CMIP5 and older) generations of Earth system models. In particular, the Arctic shelf has a number of narrow channels, which are important for oceanic circulation. Among them are channels between the north Russian coast and nearby islands and the channels in the Canadian Archipelago. The typical width of these channels is up to several tens of kilometers. Moreover, the oceanic Rossby radius, which determines the horizontal eddy scale, is $\leq$10 km at the Arctic shelf [10]. All this necessitates a very high resolution for the oceanic module in the Arctic. Ideally, this resolution should be as fine as a few kilometers [11], but such a resolution remains unfeasible for centennial- and millennial-scale simulations with Earth system models (ESMs).

The above-mentioned seafloor warming in the Laptev Sea in the last decades was reproduced in a numerical experiment using a high-resolution Arctic Ocean model and taking into account heat transport by the Lena River [12]. In this simulation, an enhanced vertical mixing in the coastal zone over the Arctic shelf was obtained, which led to the penetration of heat down to the seafloor.

In turn, knowledge of the seafloor temperature T_B is necessary to assess possible responses of the thermophysical properties of the subsea sediments to ongoing and future warming. Among these properties are the dynamics of the permafrost in the Arctic shelf [13] and the permafrost-associated methane hydrates [14,15]. Both are formed during the Pleistocene glaciations, when the shelf top (or the contemporary seafloor) was exposed to a cold atmosphere. In turn, during oceanic transgressions, the thermal regime of permafrost in the shallow Arctic shelves is mainly determined by the temperature of the overlying water layer. Thus, the measured methane release from the Arctic Ocean shelf to the atmosphere [16] allows one to assume that permafrost degrades and that methane hydrates dissociate. At present, a marked impact of the ongoing, mostly anthropogenically induced, climate warming on this release is unlikely, because of the long, multi-millennium scales of the response of the above-mentioned properties to T_B changes [17–21]. However, one could not exclude such impacts in the future, as the ongoing, mostly anthropogenically–induced, climate warming will likely progress further.

Furthermore, the fate of the methane, which is released into the oceanic water, depends on the solubility of this gas. This solubility, in turn, depends on water temperature. For instance, it was measured that the seasonal warming of the oceanic mixed layer leads

to the suppression of the methane storage capacity in water [22]. The latter suppression may increase the amount methane that is eventually emitted from the Arctic Ocean into the atmosphere.

In addition, oceanic warming over the Arctic shelf could impact Arctic ecosystems, which became more productive during recent decades [23]. Temperature changes may impact this production via two mechanisms. The first mechanism is an enhanced plankton metabolism in warmer water. The second mechanism is due to the associated changes in the oceanic stratification: an increased stratification suppresses the nutrient input for oceanic plankton, and a decreased stratification enhances it. It is clear that relative changes of the seafloor and oceanic surface temperatures might contribute to both these mechanisms.

Again, while the spatial resolution of the contemporary generation of Earth system models (ESMs) is still insufficient to resolve small-scale oceanic circulation at the Arctic shelf, this resolution has become markedly finer during the last years. In particular, it increased several fold from the CMIP3 ESMs to CMIP6 (cf. Table 8.1 in [24] and Table AnII.5 in [8]). The CMIP6 models are able to resolve the major channels in the Arctic. Thus, it is at least instructive to relate changes of the seafloor temperature to changes in surface air temperature for this ESM generation.

Long-term observations of T_B are rare or even do not exist, except those reported in [9] (V.V. Ivanov, personal communication). Thus, at present, the only way to estimate such relationships is by employing climate models. One has to take into account that, in order to make the results "climatically relevant", the simulations to be studied should fulfill the following criteria: (i) their length should be at least century scale, (ii) they should characterize climate states that are sufficiently different from the present day state, and (iii) they should be non-stationary to represent climate inertia owing to the above-mentioned dependence of the ratio between surface air and seafloor temperature changes.

The goal of the present paper was to estimate the relationship between SAT and T_B changes from the CMIP6 output for the high-emission scenario. This output fulfills all the previously mentioned criteria, and considering the previously unexamined relationships between temperature changes in the atmosphere over the Arctic shelf and near the seafloor at the same shelf.

We note that, to date, the models belonging to the CMIP6 generation have not been examined for the relationship between surface air temperature changes and the associated temperature changes near the seafloor (see above). Thus, taking into account the increased horizontal resolution of this model generation relative to the previous ones and a general interest in studying changes in the Arctic, it was appropriate to pursue the above-mentioned goals. In addition, we used simulations extended till the year 2300, which is potentially important for studying changes of the ocean—an inertial component of the Earth system.

2. Materials and Methods

We based our analysis on two variables in the CMIP annual mean output: the surface air temperature (CMIP variable *tas*) and seafloor oceanic temperature (CMIP variable *tob*). Hereafter, these two variables are denoted as T_a and T_B, correspondingly. As it is beneficial from a statistical point of view to study "large" changes, we limited ourselves to the CMIP6 historical simulations and to simulations following the Shared Socioeconomic Pathway 5-8.5 (SSP5-8.5) scenario, which is a simulation with a high CO_2 atmospheric content and is similar to the RCP8.5 scenario [25]. In addition, because our analysis was focused on very long-term applications, we limited our analysis to only the models that provide simulations until the year 2300. These models are listed in Table 1. Below, the model names are shortened, leaving only the major parts of the names, for brevity.

Table 1. CMIP6 models employed in this study.

Model	Oceanic Module	Sea Ice Module	Oceanic Resolution	ECS, °C	Reference
ACCESS-ESM1-5	ACCESS-OM2	CICE4.1	17 km, L50	3.9	[26]
CanESM5	NEMO 3.4.1	LIM2	17 km, L45	5.6	[27]
CESM2-WACCM	POP2	CICE5.1	15 km, L60	4.8	[28]
IPSL-CM6A-LR	NEMO 3.6	NEMO–LIM3	17 km, L30	4.6	[29]
MRI-ESM2-0	MRI.COM4.4	MRI.COM4.4	15 km, L61	3.2	[30]

In the "oceanic resolution" column, the first value corresponds to horizontal resolution, and the second signifies the number of vertical levels. Horizontal resolution is based on Table AII.5 from [8] but recalculated for the Arctic shelf by multiplying the values by $\cos(80^\circ)/\cos(45^\circ)$. ECS is an equilibrium climate sensitivity. ECS values were obtained from [31].

Before the analysis, both variables were reprojected onto a Cartesian $1^\circ \times 1^\circ$ grid. The interpolation weights were made proportional to $\exp(-\rho/\rho^{(0)})$, where ρ is a horizontal distance (in units of degrees of latitude and longitude) between points at two grids, and only four neighboring grid points are employed in the interpolation routine. The constant $\rho^{(0)}$ is spatially dependent, but in the Arctic it is close to 0.36°. Then, both T_a and T_B were averaged over the calendar years 1850–1900, 2005–2015, 2090–2100, and 2290–2300. Hereafter, these four time intervals are denoted as I_0, I_1, I_2, and I_3, correspondingly. Furthermore, we use the term "transition" to refer to changes of T_a and T_B between these time intervals. The relationship between changes in surface air temperature and near-floor oceanic temperature is quantified via a unit-less coefficient:

$$\alpha_j = \frac{T_{B,j} - T_{B,0}}{T_{a,j} - T_{a,0}}, \quad (1)$$

where subscript $0 \le j \le 3$ indicates the mean over the respective time interval I_j. The statistical significance of our estimate was estimated using the two-tailed Student criterion [32]. All calculated values of α appeared to be statistically significant. Therefore, the issue of this significance is not discussed thereafter. Below, the subscript j may be dropped, provided this does not lead to confusion.

We also calculated α for T_B and T_a averaged over large shelf regions: the Barents Sea (BS), the rest of Eurasia (RoE), and North America (NA), see Appendix A. Such a subdivision of Arctic shelves is somewhat untypical; basically, the Barents and Kara Seas are combined into the same sector [33–40]. We chose to average over the Barents Sea individually, because the sensitivity coefficients over this sea are very different from those over other Arctic shelves (see below). While these coefficients over the Kara Sea stand out somewhat from those over other Arctic shelves, this difference is not so pronounced relative to that exhibited over the Barents Sea. Thus, to keep the presentation compact, we merged the Kara, Laptev, and East Siberian Sea shelves into a single region for averaging.

In the latter averaging, we tried two threshold depths to mark the shelf boundaries: 200 and 500 m. The former is a typical definition of the shelf [41]. However, thus defined, the shelf appears too narrow in its meridional extent for the Barents Sea. This is the reason why we deliberately selected the latter value as well. The calculated sensitivity coefficients were very close to each other (with maximum differences of few per cents) for the two above-mentioned threshold depths for all shelves, except for the Barents Sea. Thereafter, we only present the α values, which were calculated from the averaged T_B and T_a for a threshold depth of 500 m.

Basically, the selected models reasonably reproduced surface air temperature T_a over the Arctic shelf in comparison to the reanalyses of the NCEP–DOE (National Center for Atmospheric Research–Department of Energy) [42] and ERA5 (European Centre for Medium-Range Weather Forecast Reanalysis 5) [43], with an error which is within a few degrees centigrade (Figure 1; see also Figure A2 which zooms the years 1950–2020). Thus, these models could be used for our purpose. However, because of the almost two-fold differences in their climate sensitivities (Table 1), they projected quite different regional scale SAT increases in the 21st–23rd centuries. We consider the latter as an additional benefit of our ensemble, because our models sample one of the major uncertainties in climate studies—the uncertainty due to the climate sensitivity to external forcing.

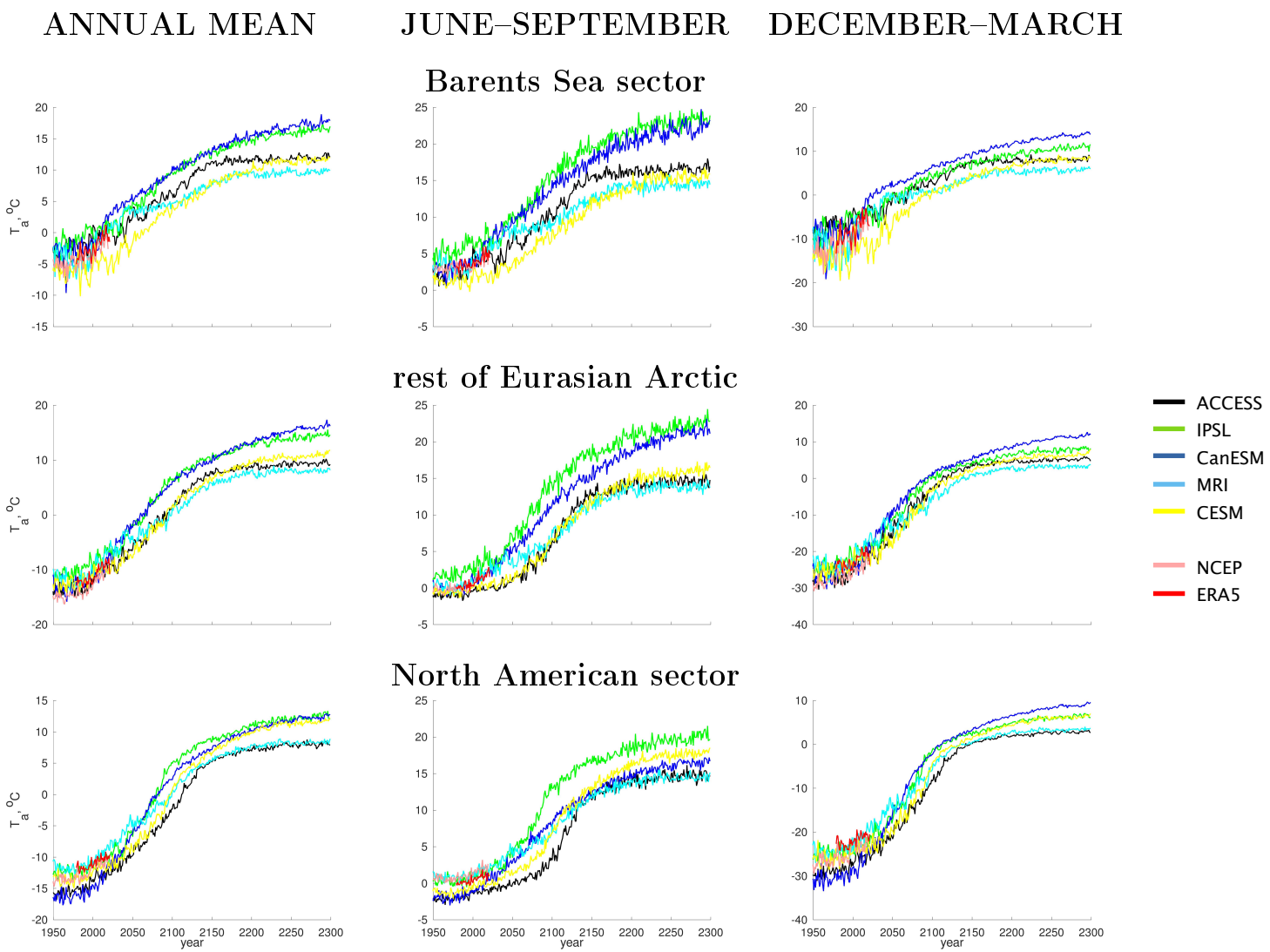

Figure 1. The shelf region-averaged surface air temperature in CMIP6 models in comparison to the NCEP–DOE and ERA5 reanalysis. The threshold depth (see text) is 500 m.

3. Results

For the annual mean temperature and transition $I_0 \rightarrow I_1$, the sensitivity coefficient α was from 0.2 to 0.9 in the Barents Sea for all models (Figure 2). The model with the maximum sensitivity coefficient was CanESM and that with the smallest was CESM. In the other shelf basins, $\alpha \leq 0.2$. The latter is consistent with the common wisdom that T_B is close-to-constant.

The coefficients α for the annual mean temperature increased markedly for $I_0 \rightarrow I_2$. In particular, the difference in the surface air and near-seafloor temperatures in CanESM and MRI was above unity near Scandinavia. Over other Arctic shelves, the α_2 was from 0.1 to 0.5 in all models.

The sensitivity coefficients for the annual mean temperatures increased further for the transition $I_0 \rightarrow I_3$. Here, three out of five models exhibited an $\alpha_3 > 1$ over the Barents Sea. This coefficient was above 0.5 over the Kara Sea. CanESM also simulated $\alpha_3 > 0.5$ over most of the Arctic shelf area. The other models simulated the values of this coefficient, which were slightly smaller over the East Siberian and North American shelves.

For the annual mean temperatures averaged over the Barents Sea region, the α_1 was from 0.14 to 0.44, depending on the model. The respective range for α_2 was from 0.32 to 0.68, and for α_3 it was from 0.62 to 0.97 (Figure 3). Over other shelf regions, the corresponding α_1 was from 0 to 0.12, α_2 was from 0.16 to 0.33, and α_3 was from 0.34 to 0.61.

For the summer (from June to September; this definition is identical to that used in [9]), the sensitivity coefficients were even larger than those obtained for the annual means (Figures 3 and 4). For the transition $I_0 \rightarrow I_1$, the maximum values of α_1 were similar to those obtained for the annual mean temperatures and were again located in the Barents Sea. However, the region with $\alpha_1 \leq 0.7$ was markedly larger than was found for the annual mean temperatures. Moreover, for all models except IPSL, regions with such large α were found over the rest of Eurasia. These regions were most pronounced in the CanESM model.

When averaged over large shelf regions, the α_1, depending on model, was from 0.28 to 0.62 in the Barents Sea sector, from 0.18 to 0.43 over RoE, and $\leq$0.30 over NA. The Barents Sea sector values were basically consistent with those derived for the inner shelf from [9].

For transitions $I_0 \rightarrow I_2$ and, especially for $I_0 \rightarrow I_3$, the sensitivity coefficients became much larger relative to those for the historical period $I_0 \rightarrow I_1$. In particular, for $I_0 \rightarrow I_2$, 3 out of 5 models simulated $\alpha > 0.7$ over vast areas of the Eurasian (both BS and RoE) shelf. This was especially marked for CanESM. Interestingly, with the ACCESS and CESM models, α_2 in the Laptev and East Siberian Seas was even larger than its counterpart in the Barents Sea. The sensitivity coefficients increased further for the transition $I_0 \rightarrow I_3$. Here, all 5 models simulated $\alpha > 0.5$ everywhere over the Arctic shelf.

For the transitions $I_0 \rightarrow I_2$ and $I_0 \rightarrow I_3$, in this season, the Barents Sea sector was not so much different from the other two sectors. For example, the area-averaged values of α_2 were from 0.51 to 0.80 in the Barents Sea sector, from 0.35 to 0.72 in RoE, and from 0.26 to 0.49 in the North American sector. The values of α_3 were from 0.65 to 1.03, from 0.57 to 0.84, and from 0.47 to 0.96, correspondingly (Figure 3).

In winter (from December to March), the sensitivity coefficients were much smaller than in summer for all models and for all time intervals (Figure 5). These coefficients were from 0.5 to 1.2 in the Barents Sea sector and always below 0.5 over the other Arctic shelves (Figure 5). Nonetheless, they still markedly increased for the transition $I_0 \rightarrow I_3$ relative to $I_0 \rightarrow I_1$ and $I_0 \rightarrow I_2$.

One may consider T_B as a function of T_a. It is clear that this function should depend on the region, on the season, on the calendar year, and on the model. However, for the shelf region-averaged values, the slope of this function showed features that were basically independent from all the above mentioned factors. Namely, this slope was very flat for temperatures below the freezing temperature of the oceanic water and it became much steeper above this temperature (see Figure 6 for annual mean values as an example). In the latter case, this slope stayed close to unity for all the models studied here. Thus, we may

hypothesize that the marked increase of our sensitivity coefficients occurred when the shelf region became ice-free in the summer.

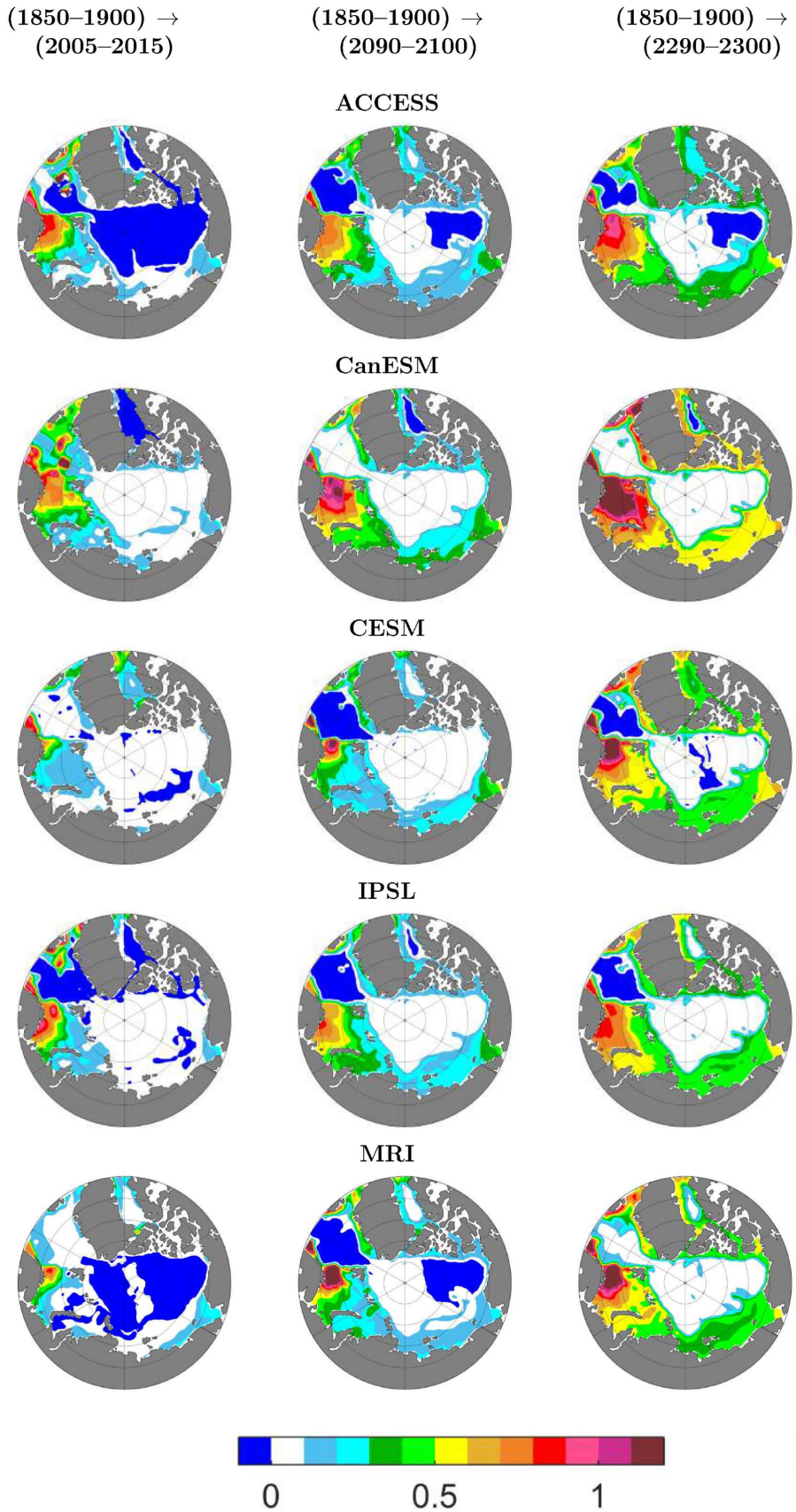

Figure 2. Coefficients α (unit-less) for annual mean temperatures and for the indicated time intervals.

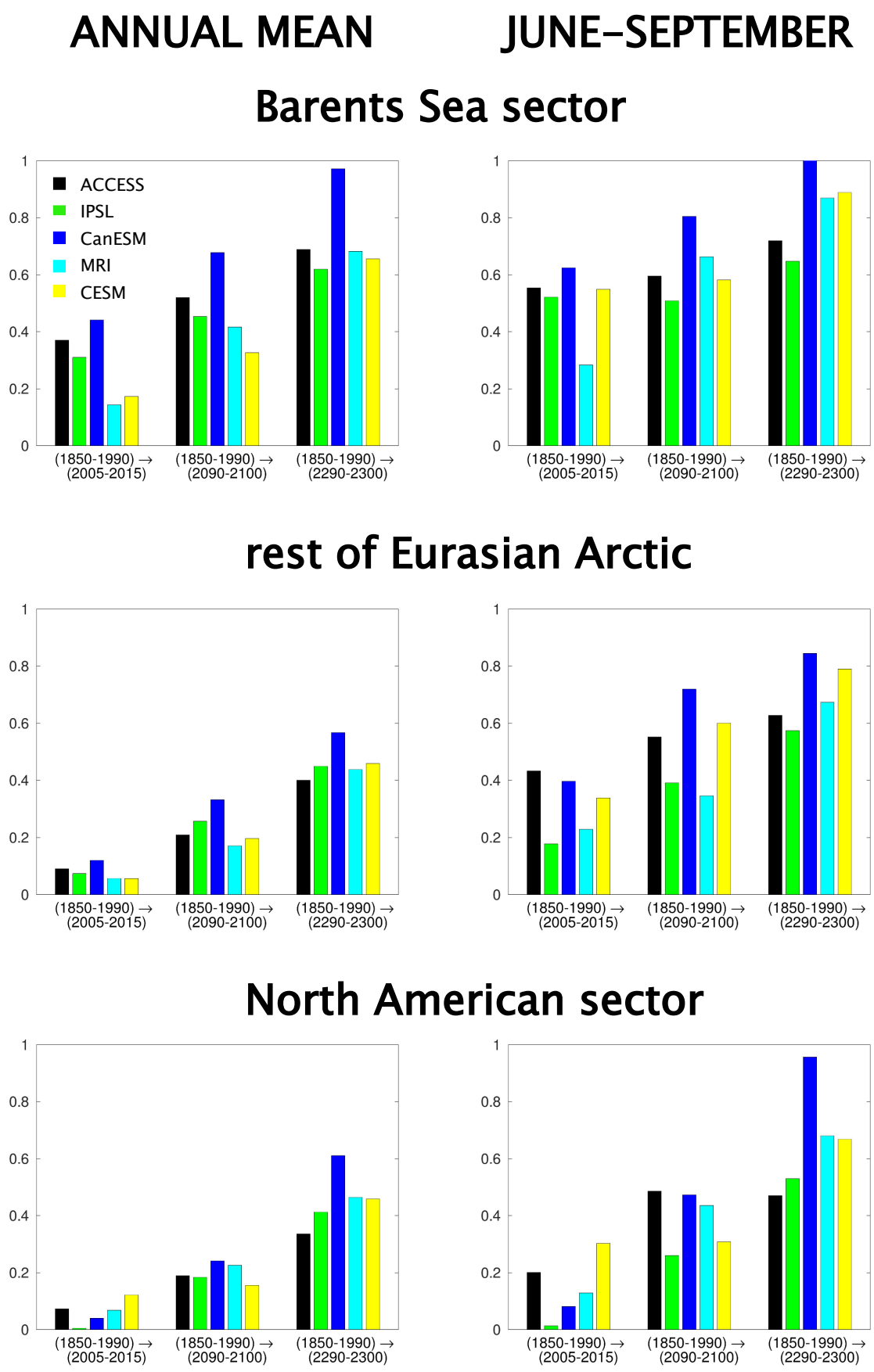

Figure 3. Coefficients α (unit-less) for annual mean temperatures (**left**) and mean June–September temperatures (**right**) averaged over the Arctic regions indicated in Figure A1.

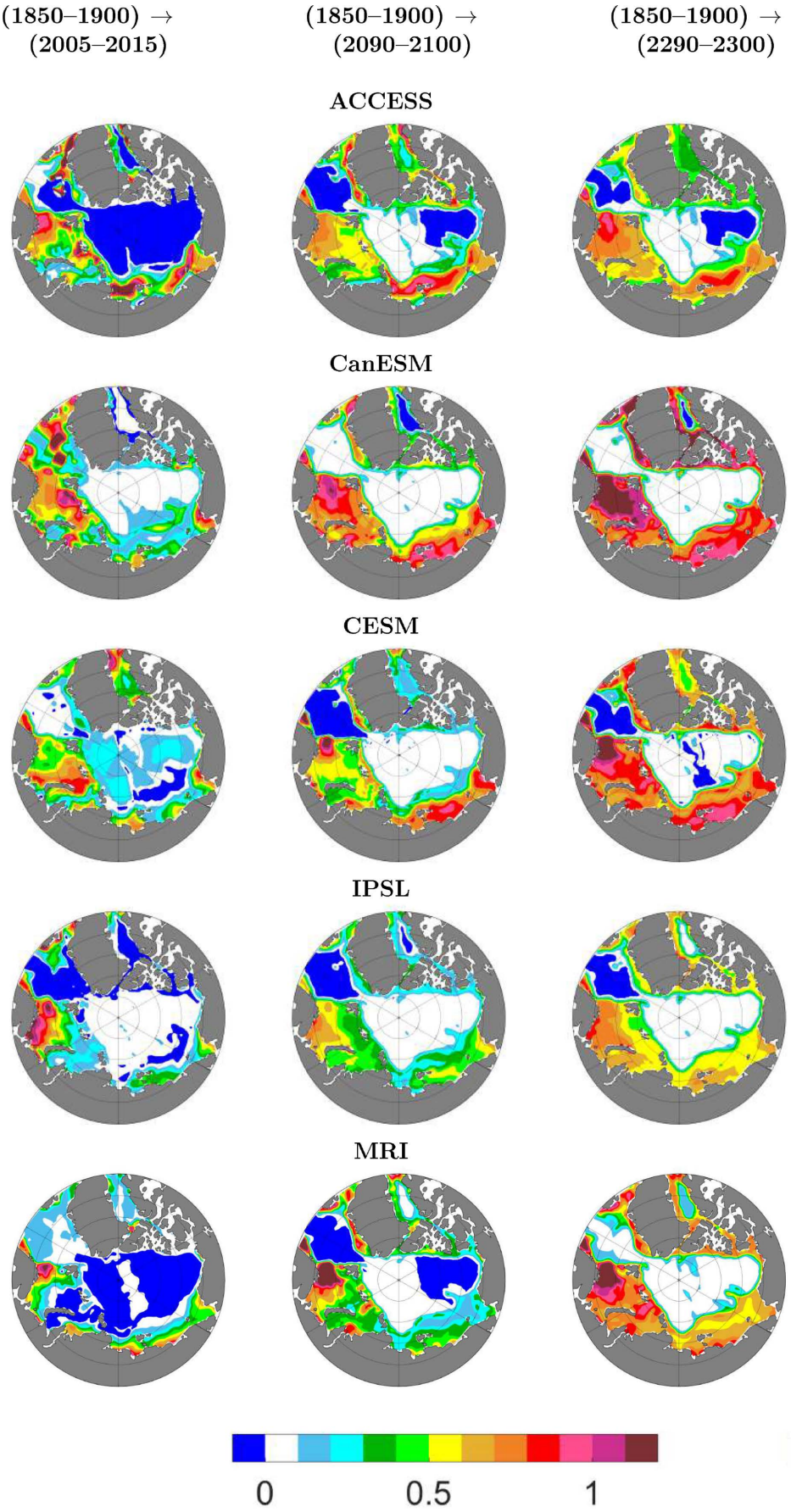

Figure 4. Similar to Figure 2, but for temperature averaged over June–September.

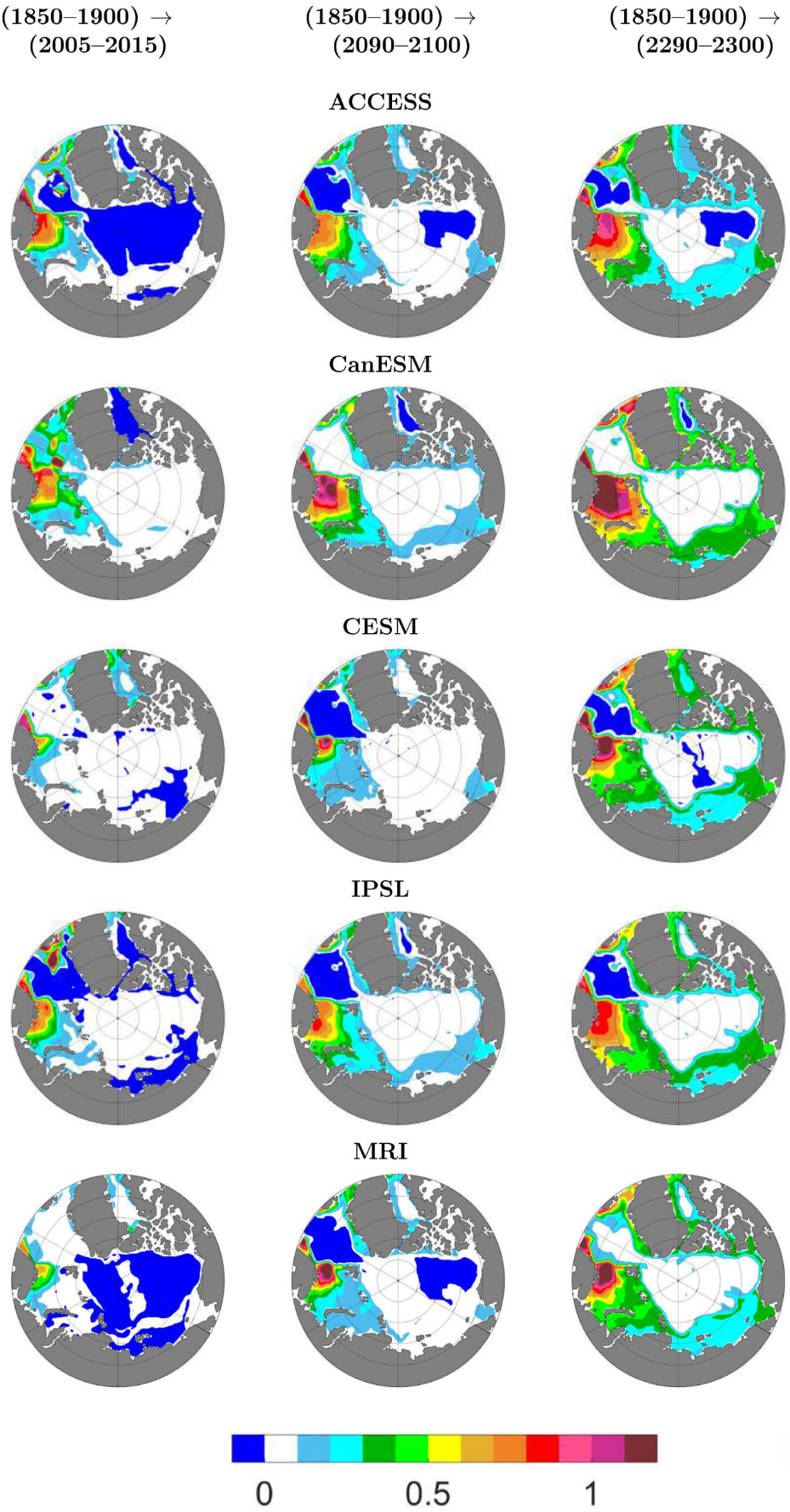

Figure 5. Similar to Figure 2, but for temperature averaged over December–March.

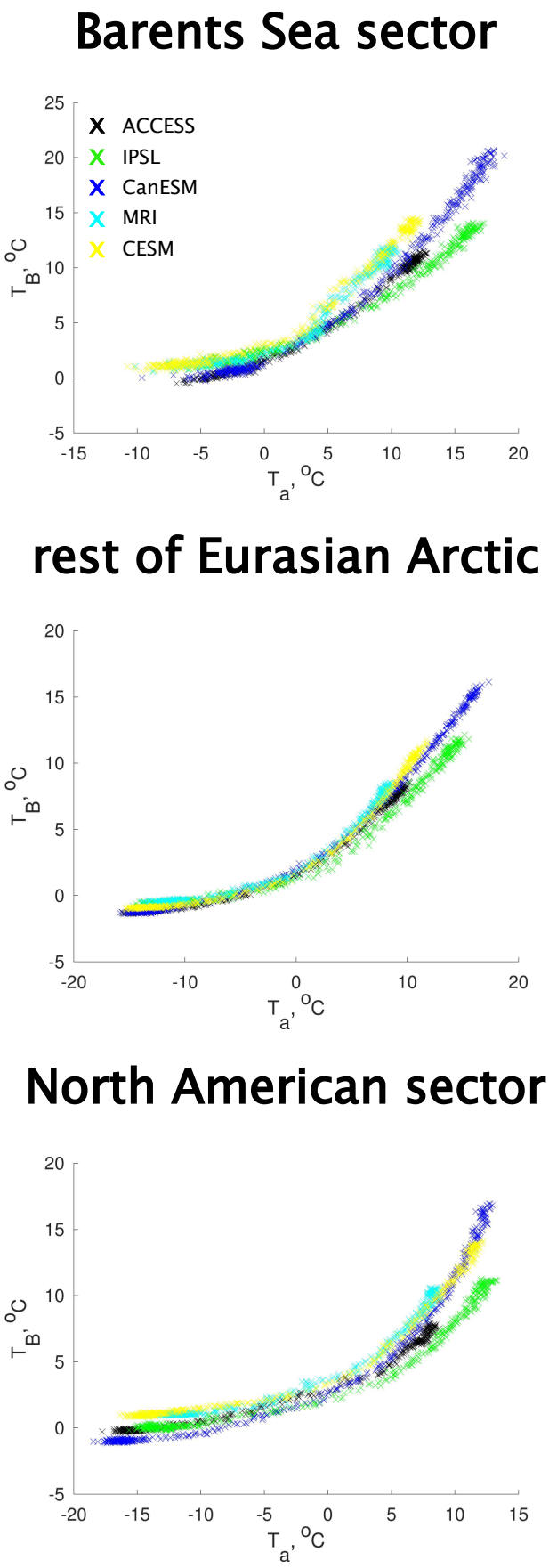

Figure 6. Annual mean T_B averaged over Arctic shelf regions as a function of the respective T_a. The threshold depth (see text) is 500 m.

Therefore, the largest sensitivity coefficient values were found in the Barents Sea. Here, they could be even larger then unity, as this was exhibited for a number of models. In other regions, the values were smaller, and sometimes they were negative. Another important feature of the calculated sensitivity coefficients was that their magnitude generally increased as time progressed.

We note that for the deep Arctic basins, there were regions with negative values of α, which were most pronounced for the ACCESS and MRI models (Figures 2, 4 and 5). The area of these regions for a given model was basically independent of season. When time progressed, both their areas and the respective spatial negative extrema diminished. While we lack a solid explanation for the occurrence of such regions, we speculate that this cooling was a manifestation of the incompletely equilibrated initial conditions for the employed model simulations. This incomplete equilibration was absent at the oceanic surface, but it was still visible at greater oceanic depths, which required infeasibly long control runs to equilibrate. The impact of the non-equailibrated initial conditions might have been additionally exacerbated by the sinking of cold water to the seafloor. Our speculation could be either proved or disproved by studying control pre-industrial runs with the same models, but this task is beyond the scope of the present paper.

4. Discussion and Conclusions

In this paper, the sensitivity of the sea-floor temperature to global warming was examined for 1850–2300, based on five CMIP6 models. This sensitivity was quantified via the ratio of changes of oceanic temperature near the seafloor, ΔT_{B}, and the surface air temperature, ΔT_{a}: $\alpha = \Delta T_{\mathrm{B}}/\Delta T_{\mathrm{a}}$. Both changes were calculated as differences of the means of the respective variable between pre-chosen time intervals. These intervals characterized the pre-industrial state (1850–1900), the present day (2005–2015), the late 21st century (2090–2100), and the late 23rd century (2290–2300). We limited ourselves by studying scenario SSP5-8.5 (Shared Socio-economic Pathways 5-8.5) with high anthropogenic emissions of greenhouse gases.

We found that, in the historical period (from 1850 to 2015), the sensitivity coefficients were rather small (typically, depending on model, $\leq$0.12 for annual means and up to 0.43 in summer). This was found irrespective of which part of the annual cycle was explored: annual means, summer means (from June to September), or winter means (from December to February). The only exception was in the Barents Sea sector, where the α was 0.14 to 0.44 for annual means, and it was from 0.28 to 0.62 for the summer means. For summer, the obtained results consistent with the limited measurements at the Siberian shelf.

For the future, sensitivity coefficients increased markedly. This was most visible in summer over the RoE sector, where the area-averaged values of sensitivity coefficients were up to 0.72, depending on model for the state change from the pre-industrial to the late 21st century, and up to 0.84 for the state change from the pre-industrial to the late 23rd century. For the latter state change, the summer sensitivity coefficient in the Barents Sea sector was very close to unity.

The most unexpected result of our paper was that sensitivity coefficient values markedly larger than 0.5 were not uncommon for this and the next few centuries. We found that such large values of α spatially coincided with the areas of most marked sea ice retreat under climate warming. In particular, during the satellite era (since 1979), the sea ice concentration in the Barents Sea has typically been below 20%, with a rapid loss in spring (see Figure 9.13 from [8]). This was accompanied by large values of α during the historical period. In late summer, the whole Arctic shelf is projected to be free of ice from approximately mid-21st century ([44] and Figure 9.13 from [8]). Thus, despite an elaborate study of Arctic sea ice being beyond the scope of the present paper, we still could conclude that our large values of α were co-incident with ice-free areas and seasons.

We might speculate that the complete melting of the sea ice in summer in a given region would lead to some freshening of the oceanic water, thus disturbing the stratification and, plausibly, enhancing the vertical mixing. The shoaling of the mixing depth is likely

to be largest in early autumn. Then, such a thick mixing layer would persist for a part of the winter, providing heat transport to the shelf seafloor. This is consistent with the results reported in [12,45]. In the former paper, it was found that, in a high-resolution coupled model, the strong increase of CO_2 content in the atmosphere leads to very deep mixing in the Arctic Ocean, including the shelf regions.

An additional possible mechanism could be the warming of the water column by solar radiation, which is absorbed directly by the water under ice-free conditions.

We may compare our results with the previous CMIP5 generation of models which participated in the Coupled Models Intercomparison Project and were driven using the Representative Concentration Pathways (RCP) 8.5 scenario until the year 2100 [6]. This scenario is quite similar to that employed in the present paper, SSP5-8.5. Using the values for ΔT_a and ΔT_B, which are listed in Introduction, we estimated $\alpha \approx 0.2$–0.3 for the transition from 2081–2100 to 1986–2005. This value is comparable to our α_2, despite the difference in the threshold depth (500 m in our paper and 1000 m in [6]). Moreover, the CMIP5-simulated change of T_B was largest in the Barents Sea sector, which is consistent with our results.

We may highlight possible applications of our results. The first application is related to changes of the thermophysical properties in the shelf sediments. If the warming at the oceanic surface leads to a non-negligible warming at the seafloor, the temperature signal has the potential to propagate into the sediment interior. After some delay (which, however, could be as long as several kiloyears [17,19,20]), this temperature signal leads to the thawing of the permafrost, which was submerged after the last glacial maximum. Furthermore, this propagating signal may lead to the dissociation of the permafrost-associated methane hydrates with a respective release of methane from the sediments to the oceanic water. In addition, the warming of the whole oceanic column over the shelf might suppress the solubility of methane in the water [22] and, therefore, increase further the release of CH_4 from the Arctic Ocean into the atmosphere.

The second application is due to the aforementioned impact of the Arctic climate changes on oceanic plankton productivity. Our cases with the close-to-unity values of α correspond to the small contribution of the temperature changes to the oceanic stratification. Thus, in these cases, this mechanism does not markedly affect the availability of nutrients for the oceanic plankton over the Arctic shelf. However, this is different for the cases with values of α that are markedly smaller than unity. In summer, when plankton blooms, the oceanic surface is generally warmer than the water near the seafloor, and the oceanic stratification is stable. Thus, $\alpha < 1$ further enhances this stability. In principle, the latter improves the availability of nutrients for plankton and, therefore, contributes to the observed amplification of the summer plankton bloom. However, our results show that this contribution could cease when the ongoing summer ice loss has progressed sufficiently. We note, however, that both mechanisms—an increase of nutrient availability until the sea ice loss has sufficiently progressed and a negligible impact when this progression has occurred—are likely to be modified by salinity effects.

Our paper has some limitations. The first is due to the coarse horizontal resolution of the employed CMIP6 models, which still cannot resolve individual eddies in the Arctic Ocean. Thus, small-scale circulations in the ocean, which have the potential to transport sensible heat downward in the water column, are lacking in the CMIP6 model generation.

Another limitation is due to the small size of the employed ensemble. This size was determined by the availability of simulations. As our sensitivity coefficients depend on the model, we acknowledge that any additional models would change our results to some extent. However, the summer sea ice loss in the 21st century is common to all CMIP6 models and even to all CMIP6 scenarios [44]. Thus, one may safely state that close-to-unity sensitivity coefficients would be exhibited over the Arctic shelf provided that warming has sufficiently progressed and the summer sea ice has melted in a region of interest.

Furthermore, we only studied the model output in the simulations forced by the SSP5-8.5 scenario. Certainly, for our preselected time intervals, the sensitivity coefficients for other scenarios would be different. However, the major point of our paper was the

strong increase of such coefficients in the regions that are ice-free in summer. In this respect, the most important point is whether a given climate scenario would lead to a complete melting of ice in summer in the region under study. We believe that this result is applicable to other scenarios as well, provided that the respective warming is strong enough to lead to such melting.

Next, despite claiming a strong dependence of the sensitivity coefficient on the state of sea ice, we did not make an attempt to construct an explicit relationship for α with ice concentration. We chose this approach because such a relationship is likely to be non-local (due to the influence of oceanic circulation on T_B). The response of near-floor temperature at the shelf is likely to be delayed with respect to sea ice changes, which complicates a construction of this relationship. Moreover, our principal interest in future applications of the results of the present paper is to study the thermophysics of the shelf sediments at millennium and multi-millennium scales. Since, again, the Arctic shelf is expected to become ice-free in summer from the middle of the 21st century until the warming is sufficiently reversed for the ice cover to be recovered, the majority of the respective simulations could be performed under ice-free conditions in summer and, therefore, with "asimptotically high" (in terms of vanishing sea ice concentration) sensitivity coefficients.

Finally, we note the results for the end of this century and for longer periods should be considered with caution, since small changes in the variables may provide varied results at the end of extended periods. However, the major result that the sensitivity coefficients α will become close to unity when the Arctic becomes seasonally ice-free is model independent. Thus, it may be considered reliable.

Despite all the above-mentioned limitations, we conclude that it is not unrealistic to assume, for millennium- and multi-millennium–scale projections of the thermophysical state of the Arctic shelf sediments, that the near-floor warming will be of the same order of magnitude as the warming of the near-surface air, provided that the latter warming is accompanied by sea ice loss.

Author Contributions: Conceptualization, V.V.M. and A.V.E.; software, V.V.M.; formal analysis, V.V.M. and A.V.E.; data curation, V.V.M.; writing—original draft preparation, A.V.E.; writing—review and editing, V.V.M. and A.V.E.; funding acquisition, A.V.E. All authors have read and agreed to the published version of the manuscript.

Funding: This research was funded and supported by the Russian Science Foundation grant 21-17-00012.

Data Availability Statement: No data were created during preparation of this paper.

Acknowledgments: The authors are indebted to V.V. Ivanov for useful discussions on oceanic measurements in the Arctic. The authors are indebted to the four anonymous reviewers, whose comments led to an improved presentation of the obtained results.

Conflicts of Interest: The authors declare no conflict of interest.

Abbreviations

The following abbreviations are used in this manuscript:

BS	Barents Sea
NA	North America/North American
RoE	Rest of Eurasia

Appendix A. Regions Used for Spatial Averaging

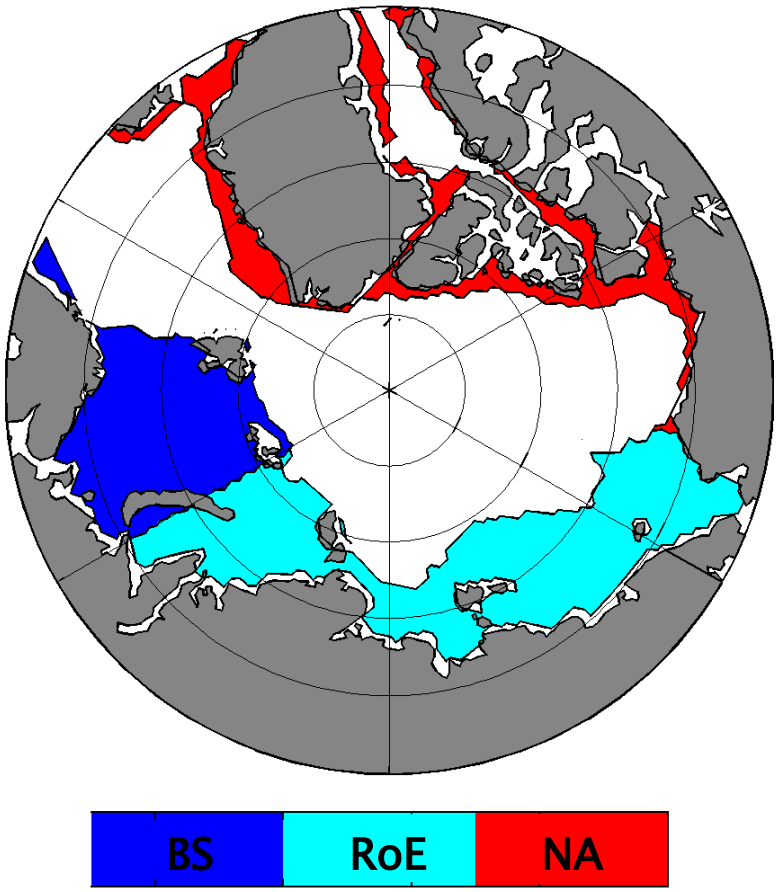

Figure A1. Mask of regions with the threshold oceanic depth of 500 m for temperature averaging.

Appendix B. Comparison of the Modeled T_a with the Reanalyses Data

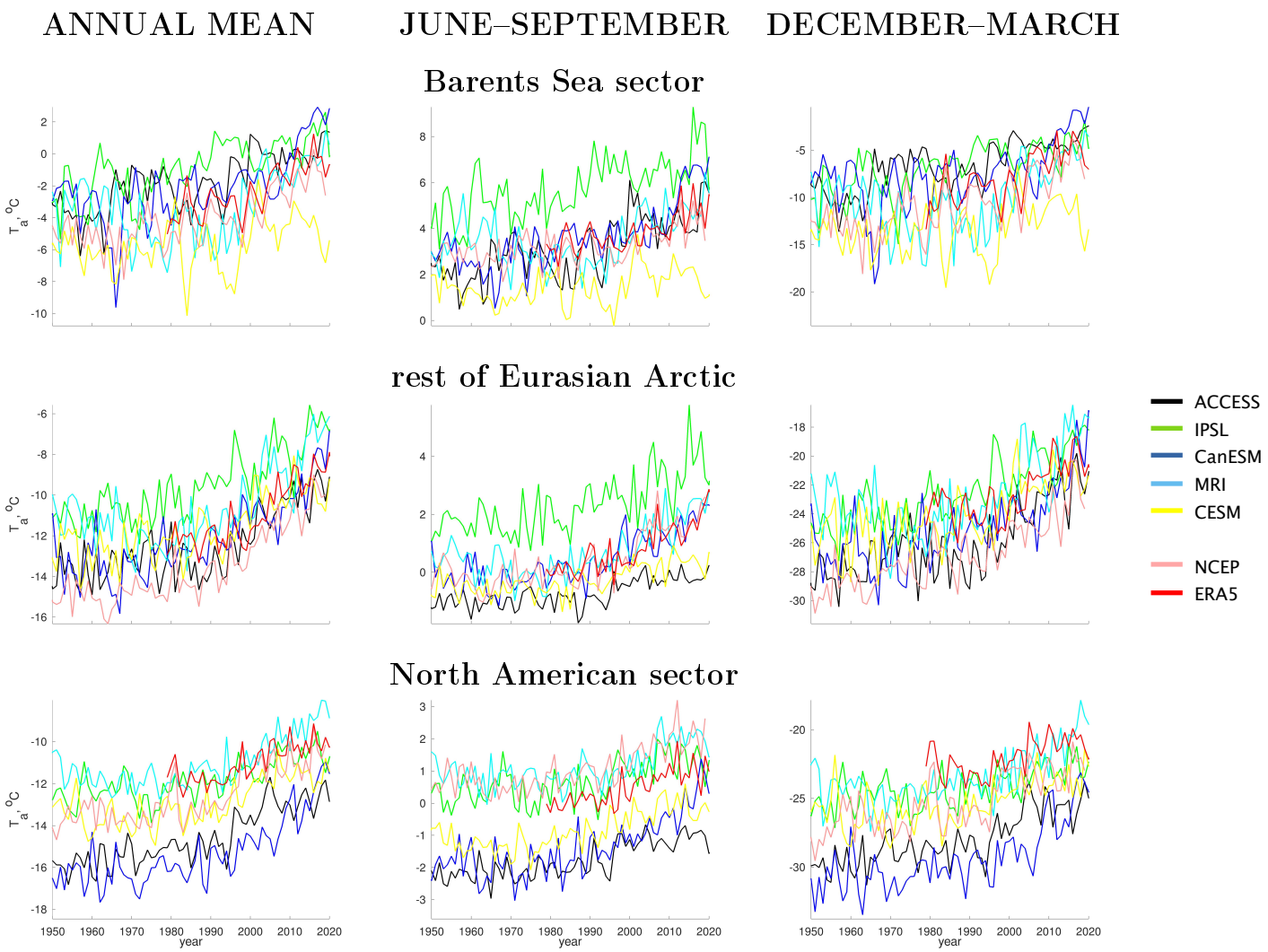

Figure A2. Similar to Figure 1 but only for 1950–2020.

References

1. Masson-Delmotte, V.; Kageyama, M.; Braconnot, P.; Charbit, S.; Krinner, G.; Ritz, C.; Guilyardi, E.; Jouzel, J.; Abe-Ouchi, A.; Cruci, M.; et al. Past and future polar amplification of climate change: Climate model intercomparisons and ice–core constraints. *Clim. Dyn.* **2006**, *26*, 513–529. [CrossRef]
2. Bekryaev, R.; Polyakov, I.; Alexeev, V. Role of polar amplification in long–term surface air temperature variations and modern Arctic warming. *J. Clim.* **2010**, *23*, 3888–3906. [CrossRef]
3. Previdi, M.; Smith, K.; Polvani, L. Arctic amplification of climate change: A review of underlying mechanisms. *Environ. Res. Lett.* **2021**, *16*, 093003. [CrossRef]
4. Lamarque, J.F. Estimating the potential for methane clathrate instability in the 1%-CO2 IPCC AR-4 simulations. *Geophys. Res. Lett.* **2008**, *35*, L19806. [CrossRef]
5. Collins, M.; Knutti, R.; Arblaster, J.; Dufresne, J.L.; Fichefet, T.; Friedlingstein, P.; Gao, X.; Gutowski, W.; Johns, T.; Krinner, G.; et al. Long–term climate change: Projections, commitments and irreversibility. In *Climate Change 2013: The Physical Science Basis. Contribution of Working Group I to the Fifth Assessment Report of the Intergovernmental Panel on Climate Change*; Stocker, T., Qin, D., Plattner, G.K., Tignor, M., Allen, S., Boschung, J., Nauels, A., Xia, Y., Bex, V., Midgley, P., Eds.; Cambridge University Press: Cambridge, UK; New York, NY, USA, 2013; pp. 1029–1136.
6. Heuzé, C.; Heywood, K.; Stevens, D.; Ridley, J. Changes in global ocean bottom properties and volume transports in CMIP5 models under climate change scenarios. *J. Clim.* **2015**, *28*, 2917–2944. [CrossRef]
7. Shu, Q.; Wang, Q.; Årthun, M.; Wang, S.; Song, Z.; Zhang, M.; Qiao, F. Arctic Ocean Amplification in a warming climate in CMIP6 models. *Sci. Adv.* **2022**, *8*, 30. [CrossRef]
8. Masson-Delmotte, V.; Zhai, P.; Pirani, A.; Connors, S.; Péan, C.; Berger, S.; Caud, N.; Chen, Y.; Goldfarb, L.; Gomis, M.; et al. (Eds.) *Climate Change 2021: The Physical Science Basis. Contribution of Working Group I to the Sixth Assessment Report of the Intergovernmental Panel on Climate Change*; Cambridge University Press: Cambridge, UK; New York, NY, USA, 2021; p. 2391.
9. Dmitrenko, I.; Kirillov, S.; Tremblay, L.; Kassens, H.; Anisimov, O.; Lavrov, S.; Razumov, S.; Grigoriev, M. Recent changes in shelf hydrography in the Siberian Arctic: Potential for subsea permafrost instability. *J. Geophys. Res. Ocean.* **2011**, *116*, C10027. [CrossRef]
10. Nurser, A.; Bacon, S. The Rossby radius in the Arctic Ocean. *Ocean Sci.* **2014**, *10*, 967–975. [CrossRef]
11. Wang, Q.; Wekerle, C.; Danilov, S.; Wang, X.; Jung, T. A 4.5 km resolution Arctic Ocean simulation with the global multi–resolution model FESOM 1.4. *Geosci. Model. Dev.* **2018**, *11*, 1229–1255. [CrossRef]
12. Golubeva, E.; Platov, G.; Malakhova, V.; Kraineva, M.; Iakshina, D. Modelling the long-term and inter-annual variability in the Laptev Sea hydrography and subsea permafrost state. *Polarforschung* **2018**, *87*, 195–210. [CrossRef]
13. Romanovskii, N.; Hubberten, H.W. Results of permafrost modelling of the lowlands and shelf of the Laptev Sea region, Russia. *Permafr. Perigl. Proc.* **2001**, *12*, 191–202. [CrossRef]
14. O'Connor, F.; Boucher, O.; Gedney, N.; Jones, C.; Folberth, G.; Coppell, R.; Friedlingstein, P.; Collins, W.; Chappellaz, J.; Ridley, J.; et al. Possible role of wetlands, permafrost, and methane hydrates in the methane cycle under future climate change: A review. *Rev. Geophys.* **2010**, *48*, RG4005. [CrossRef]
15. Ruppel, C.; Kessler, J. The interaction of climate change and methane hydrates. *Rev. Geophys.* **2017**, *55*, 126–168. [CrossRef]
16. Shakhova, N.; Semiletov, I.; Chuvilin, E. Understanding the permafrost–hydrate system and associated methane releases in the East Siberian Arctic Shelf. *Geosciences* **2019**, *9*, 251. [CrossRef]
17. Romanovskii, N.; Hubberten, H.W.; Gavrilov, A.; Eliseeva, A.; Tipenko, G. Offshore permafrost and gas hydrate stability zone on the shelf of East Siberian Seas. *Geo-Mar. Lett.* **2005**, *25*, 167–182. [CrossRef]
18. Shakhova, N.; Semiletov, I.; Leifer, I.; Sergienko, V.; Salyuk, A.; Kosmach, D.; Chernykh, D.; Stubbs, C.; Nicolsky, D.; Tumskoy, V.; et al. Ebullition and storm-induced methane release from the East Siberian Arctic Shelf. *Nat. Geosci.* **2014**, *7*, 64–70. [CrossRef]
19. Malakhova, V.; Eliseev, A. The role of heat transfer time scale in the evolution of the subsea permafrost and associated methane hydrates stability zone during glacial cycles. *Glob. Planet. Chang.* **2017**, *157*, 18–25. [CrossRef]
20. Malakhova, V.; Eliseev, A. Uncertainty in temperature and sea level datasets for the Pleistocene glacial cycles: Implications for thermal state of the subsea sediments. *Glob. Planet. Chang.* **2020**, *192*, 103249. [CrossRef]
21. Canadell, J.; Monteiro, P.; Costa, M.; Cotrim da Cunha, L.; Cox, P.; Eliseev, A.; Henson, S.; Ishii, M.; Jaccard, S.; Koven, C.; et al. Global carbon and other biogeochemical cycles and feedbacks. In *Climate Change 2021: The Physical Science Basis. Contribution of Working Group I to the Sixth Assessment Report of the Intergovernmental Panel on Climate Change*; Masson-Delmotte, V., Zhai, P., Pirani, A., Connors, S., Péan, C., Berger, S., Caud, N., Chen, Y., Goldfarb, L., Gomis, M., et al., Eds.; Cambridge University Press: Cambridge, UK; New York, NY, USA, 2021; pp. 673–815.
22. Vinogradova, E.; Damm, E.; Pnyushkov, A.; Krumpen, T.; Ivanov, V. Shelf-sourced methane in surface seawater at the Eurasian continental slope (Arctic Ocean). *Front. Environ. Sci.* **2022**, *10*, 811375. [CrossRef]
23. Ardyna, M.; Arrigo, K. Phytoplankton dynamics in a changing Arctic Ocean. *Nat. Clim. Chang.* **2020**, *10*, 892–903. [CrossRef]
24. Solomon, S.; Qin, D.; Manning, M.; Marquis, M.; Averyt, K.; Tignor, M.; LeRoy Miller, H.; Chen, Z. (Eds.) *Climate Change 2007: The Physical Science Basis*; Cambridge University Press: Cambridge, UK; New York, NY, USA, 2007; p. 996.
25. Gidden, M.; Riahi, K.; Smith, S.; Fujimori, S.; Luderer, G.; Kriegler, E.; van Vuuren, D.; van den Berg, M.; Feng, L.; Klein, D.; et al. Global emissions pathways under different socioeconomic scenarios for use in CMIP6: A dataset of harmonized emissions trajectories through the end of the century. *Geosci. Model. Dev.* **2019**, *12*, 1443–1475. [CrossRef]

26. Ziehn, T.; Chamberlain, M.; Law, R.; Lenton, A.; Bodman, R.; Dix, M.; Stevens, L.; Wang, Y.P.; Srbinovsky, J. The Australian Earth system model: ACCESS-ESM1.5. *J. South. Hemisph. Earth Sys. Sci.* **2020**, *70*, 193–214. [CrossRef]
27. Swart, N.; Cole, J.; Kharin, V.; Lazare, M.; Scinocca, J.; Gillett, N.; Anstey, J.; Arora, V.; Christian, J.R.; Hanna, S.; et al. The Canadian Earth System Model version 5 (CanESM5.0.3). *Geosci. Model. Dev.* **2019**, *12*, 4823–4873. [CrossRef]
28. Danabasoglu, G.; Lamarque, J.F.; Bacmeister, J.; Bailey, D.; DuVivier, A.; Edwards, J.; Emmons, L.; Fasullo, J.; Garcia, R.; Gettelman, A.; et al. The Community Earth System Model Version 2 (CESM2). *J. Adv. Model. Earth Syst.* **2020**, *12*, e2019MS001916. [CrossRef]
29. Boucher, O.; Servonnat, J.; Albright, A.; Aumont, O.; Balkanski, Y.; Bastrikov, V.; Bekki, S.; Bonnet, R.; Bony, S.; Bopp, L.; et al. Presentation and Evaluation of the IPSL-CM6A-LR climate model. *J. Adv. Model. Earth Syst.* **2020**, *12*, e2019MS002010. [CrossRef]
30. Yukimoto, S.; Kawai, H.; Koshiro, T.; Oshima, N.; Yoshida, K.; Urakawa, S.; Tsujino, H.; Deushi, M.; Tanaka, T.; Hosaka, M.; et al. The Meteorological Research Institute Earth system model version 2.0, MRI–ESM2.0: Description and basic evaluation of the physical component. *J. Met. Soc. Jpn.* **2019**, *97*, 931–965. [CrossRef]
31. Meehl, G.; Senior, C.; Eyring, V.; Flato, G.; Lamarque, J.F.; Stouffer, R.; Taylor, K.; Schlund, M. Context for interpreting equilibrium climate sensitivity and transient climate response from the CMIP6 Earth system models. *Sci. Adv.* **2020**, *6*, eaba1981. [CrossRef]
32. von Storch, H.; Zwiers, F. *Statistical Analysis in Climate Research*; Cambridge University Press: Cambridge, UK, 2003; p. 484.
33. Petoukhov, V.; Semenov, V. A link between reduced Barents–Kara sea ice and cold winter extremes over northern continents. *J. Geophys. Res. Atmos.* **2010**, *115*, D21111. [CrossRef]
34. Semenov, V.; Latif, M. Nonlinear winter atmospheric circulation response to Arctic sea ice concentration anomalies for different periods during 1966–2012. *Environ. Res. Lett.* **2015**, *10*, 054020. [CrossRef]
35. Ringgaard, I.; Yang, S.; Kaas, E.; Christensen, J. Barents–Kara sea ice and European winters in EC-Earth. *Clim. Dyn.* **2020**, *54*, 3323–3338. [CrossRef]
36. Puglini, M.; Brovkin, V.; Regnier, P.; Arndt, S. Assessing the potential for non–turbulent methane escape from the East Siberian Arctic Shelf. *Biogeosciences* **2020**, *17*, 3247–3275. [CrossRef]
37. Chen, Y.; Luo, D.; Zhong, L.; Yao, Y. Effects of Barents–Kara Seas ice and North Atlantic tripole patterns on Siberian cold anomalies. *Weather Clim. Extrem.* **2021**, *34*, 100385. [CrossRef]
38. Parfenova, M.; Eliseev, A.; Mokhov, I. Changes in the duration of the navigation period in Arctic seas along the Northern Sea Route in the twenty–first century: Bayesian estimates based on calculations with the ensemble of climate models. *Dokl. Earth Sci.* **2022**, *507*, 952–958. [CrossRef]
39. Yamagami, Y.; Watanabe, M.; Mori, M.; Ono, J. Barents–Kara sea–ice decline attributed to surface warming in the Gulf Stream. *Nat. Commun.* **2022**, *13*, 3767. [CrossRef] [PubMed]
40. Komatsu, K.; Takaya, Y.; Toyoda, T.; Hasumi, H. Response of Eurasian temperature to Barents–Kara sea ice: Evaluation by multi–model seasonal predictions. *Geophys. Res. Lett.* **2022**, *49*, e2021GL097203. [CrossRef]
41. Agapova, G.; Budanova, L.; Zenkevich, N.; Larina, N.; Litvin, V.; Marova, N.; Rudenko, M.; Turko, N. Geomorphology of the oceanic floor. In *Okeanology: Oceanic Geophysics. V. 1*; Monin, A., Bezrukov, P., Bordovskii, O., Vinogradov, M., Volkov, I., Kamenkovich, V., Lisitsyn, A., Neprochnov, Y., Sorokhtin, O., Eds.; Nauka: Moscow, Russia, 1979; pp. 150–205. (In Russian)
42. Kanamitsu, M.; Ebisuzaki, W.; Woollen, J.; Yang, S.K.; Hnilo, J.; Fiorino, M.; Potter, G. NCEP–DOE AMIP-II reanalysis (R-2). *Bull. Am. Meteorol. Soc.* **2002**, *83*, 1631–1644. [CrossRef]
43. Hersbach, H.; Bell, B.; Berrisford, P.; Hirahara, S.; Horányi, A.; Muñoz-Sabater, J.; Nicolas, J.; Peubey, C.; Radu, R.; Schepers, D.; et al. The ERA5 global reanalysis. *Q. J. R. Meteorol. Soc.* **2020**, *146*, 1999–2049. [CrossRef]
44. Notz, D.; SIMIP Community. Arctic sea ice in CMIP6. *Geophys. Res. Lett.* **2020**, *47*, e2019GL086749. [CrossRef]
45. Lique, C.; Johnson, H.; Plancherel, Y. Emergence of deep convection in the Arctic Ocean under a warming climate. *Clim. Dyn.* **2018**, *50*, 3833–3847. [CrossRef]